Electronic Supplementary Material (ESI) for Materials Chemistry Frontiers.

Supporting Information

Increasing the Stability in Air of Mg_2(dobpdc) Metal-Organic Framework Through Solvent Removal

Jenny G. Vitillo,* Silvia Bordiga

Department of Chemistry, NIS Center and INSTM, University of Turin, via Gioacchino Quarello 15A, I-10135 Torino, Italy.

Content

S1. Materials and methods

Synthesis. Mg_2(dobpdc) was synthetized accordingly to the procedure reported in Ref. 1. It was then washed three times in dimethylformamide followed by three washing in methanol. It was then used as it is (**sol**) or activated in vacuum ($< 5\ 10^{-4}$ mbar) at 180°C for 15 h (**act**).

Aging measurements. The relative humidity and temperature during the aging has been measured by a thermometer-hygrometer station TFA 30.5021.02 (TFA-Dostmann, Germany). Accuracy on humidity reading was ±4% in the 35-75 RH% range, whereas at larger RH% the accuracy was lower (±>5%). Accuracy on temperature reading was ±1°C from 0 to 40°C, otherwise ±1.5°C. **act-humid** and **sol-humid** were prepared placing the **act** and **sol** samples, respectively, in a PP sample vessel in a home-made aging chamber constituted by an overturned bucket and a crystallizer filled with water, in order to create a saturated vapor atmosphere. For what concerns **act-indoor** and **sol-indoor** samples, the pristine materials were simply exposed to air in the laboratory. The temperature, relative humidity and time conditions maintained during the aging for all the materials are reported in Table 1 of the main text.

Volumetry. Nitrogen and carbon dioxide adsorption isotherms were measured on a commercial volumetric apparatus (Micromeritics ASAP2020). Prior to the measurements, the powders were degassed at RT for 60 min followed by a treatment at 180°C for 15 h on a vacuum line equipped with a turbomolecular pump and then transferred in the measurement cell in a glove box. During the N_2 measurements, the temperature was maintained at 77 K by a liquid nitrogen bath, whereas for the CO_2 ones a circulating water bath was adopted (Julabo, F25-HE). The specific surface area was obtained by using the Langmuir and B.E.T. [2, 3] method in the standard pressure range ($0.05 < p/p_0 < 0.20$). All the reported quantities are affected by an error of 10%.

XRD Powder measurements. X-Ray Powder Diffraction measurements were performed in the 2θ range 2°-60° (step size of 0.0167°, time per step 10 s) in Debye-Scherrer geometry using a laboratory diffractometer (Panalytical X'Pert Pro Multipurpose Diffractometer) having as source a high powdered ceramic tube PW3373/10 LFF with a Cu anode equipped with a Ni filter to attenuate K_{β} and focused by a PW3152/63 X-ray mirror. The incident beam was collimated by a soller slit (0.04 rad), an antiscatter slit (1/2 Å) and a divergence slit (1/2 Å); for the diffracted beam an antiscatter slit (AS Slit 5.0 mm, X'Celerator) and a soller slit (0.04 rad) were adopted. Samples were sealed into boron silica glass capillaries of internal diameter 0.8 mm in air or in a protected atmosphere and mounted on a rotating goniometer head. No difference was observed in the patterns upon rotation. For this reason, the head was left motionless in the in situ study. The ex situ patterns have been refined by means of the Pawley method as implemented in the TOPAS-Academic V5 program.

FTIR spectroscopy in trasmission. In situ FTIR spectra in transmission mode (2 cm^{-1} resolution, average on 64 scans) were collected on a Bruker Vertex70 spectrophotometer. The samples were measured in the form of self-supporting pellets inside a quartz cell in controlled atmosphere.

ATR-FTIR spectroscopy. Infrared spectra in Attenuated Total Reflection (ATR-IR) were collected on loose powder on a Bruker Alpha spectrophotometer (2 cm^{-1} resolution, average on 256 scans), equipped with an internal reflection element in diamond and placed in the glove box. The spectrum intensity was corrected for the effective thickness value for the different incident wavelengths.

S2. Mg_2(dobdc) and Mg_2(dobpdc) structures

The structures of Mg_2(dobpdc) and of its isomorph Mg_2(dobdc) are reported in Figure S1.

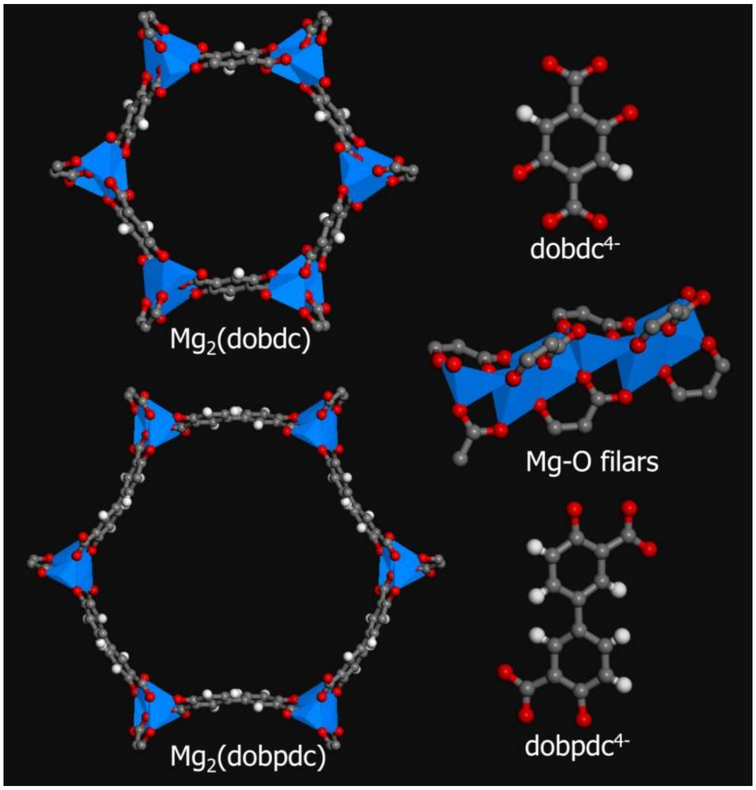

Figure S1. Atomistic representation of the Mg_2(dobdc) (also known as MOF-74-Mg) and Mg_2(dobpdc) structures. Color code: light blue (magnesium), grey (carbon), red (oxygen) and white (hydrogen).

S3. Samples color

If the material decomposed, it assumed a color after 1 h in atmospheres having < 50 RH%: in air they assumed a dark blue color whereas after activation in vacuum they became green in color (see Figure S2). In particular, **act-indoor** maintained a whitish color, whereas **sol-indoor** showed a blue coloration, turning to green during sample activation. The change in color was limited to the external and superior layer of the particles and it was observed also after degradation in the dark (see Table 1).

sol-humid maintained a white color, turning to blue after 1 h at 40 RH% and then to green after degassing in vacuum a RT.

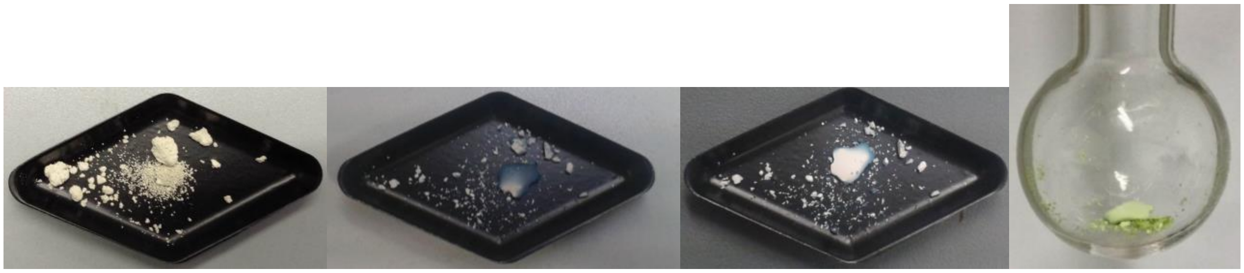

Figure S2. (from left to right) Pictures of the **sol-humid** (air, white), **sol-indoor** (air, superior part, blue), **sol-indoor** (air, inferior part, white), fully activated **sol-indoor** (vacuum, green). The lightening as cause of the blue coloration of the superior part of the sample can be ruled out being the same behavior observed for a material kept in the dark.

S4. In situ XRPD measurements for act-indoor and sol-indoor

The decomposition of sol and act samples in air for RH%<50 was monitored over time by in situ XRPD. The measured patterns are reported in Figure S3-Figure S4 for **sol** and Figure S5-Figure S6 for **act**.

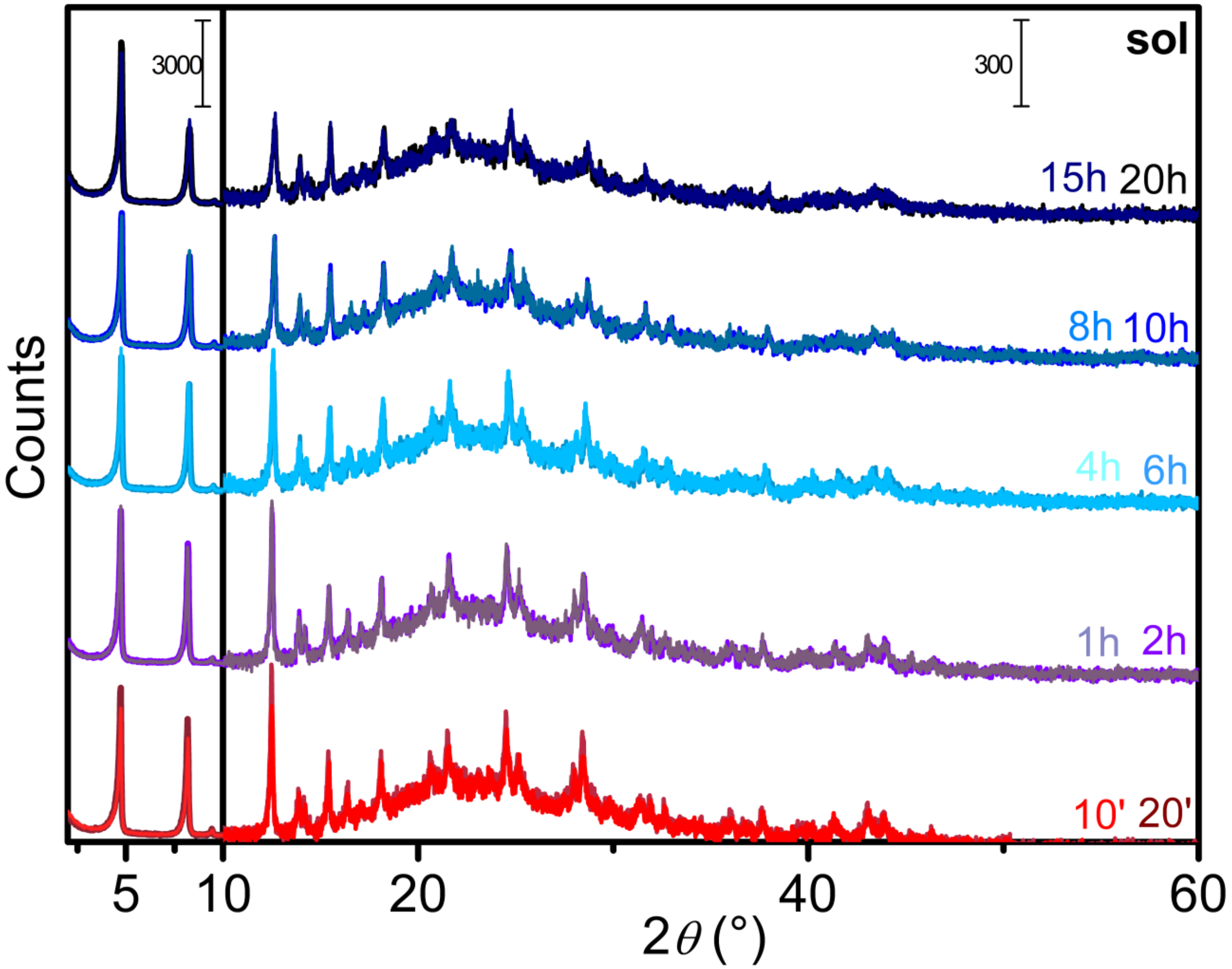

Figure S3. In situ XRD patterns recorded over time for solvated Mg_2(dobpdc) (**sol**) exposed to air (22°C, 29-40 RH%) up to 20 h (**sol-indoor**).

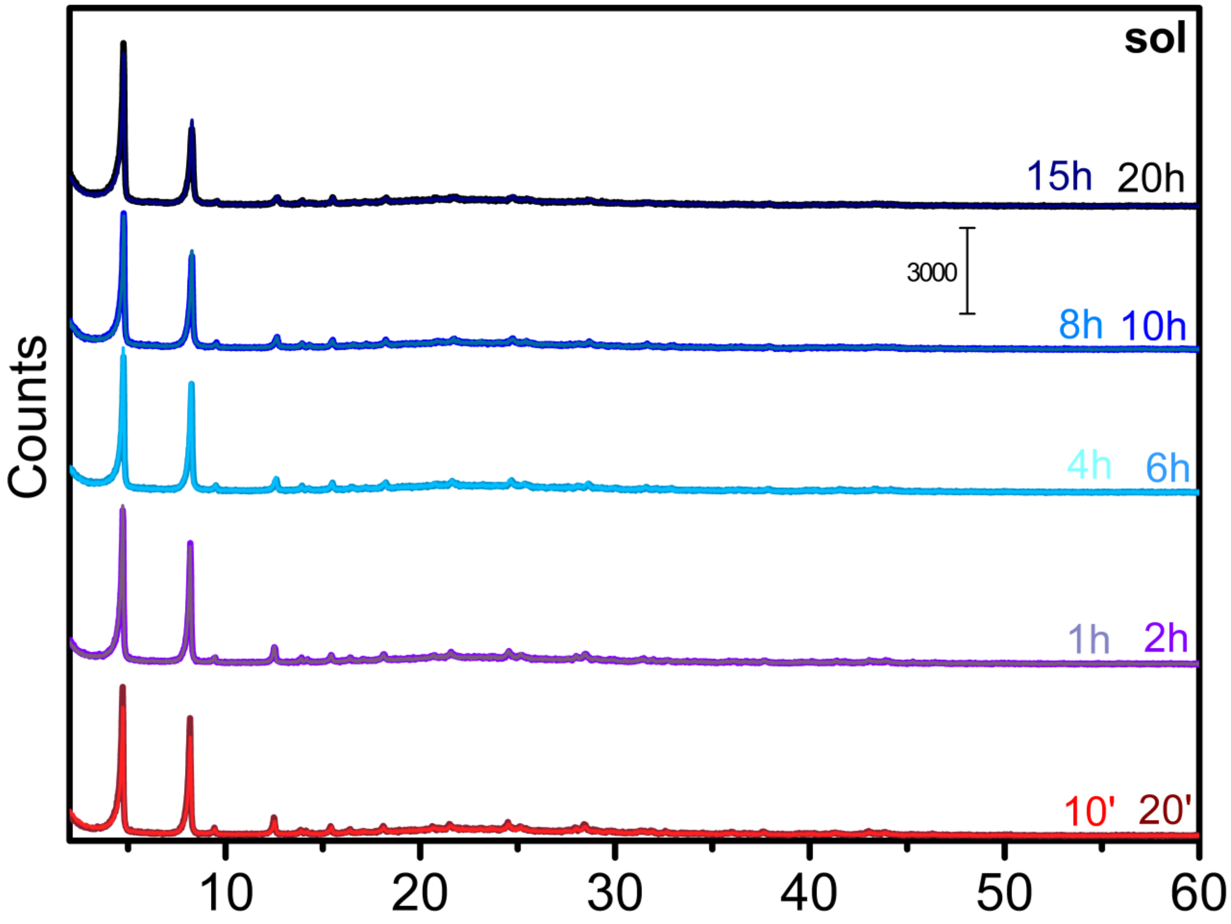

Figure S4. In situ XRD patterns reported in Figure S3 by adopting the same scale in the whole angle range.

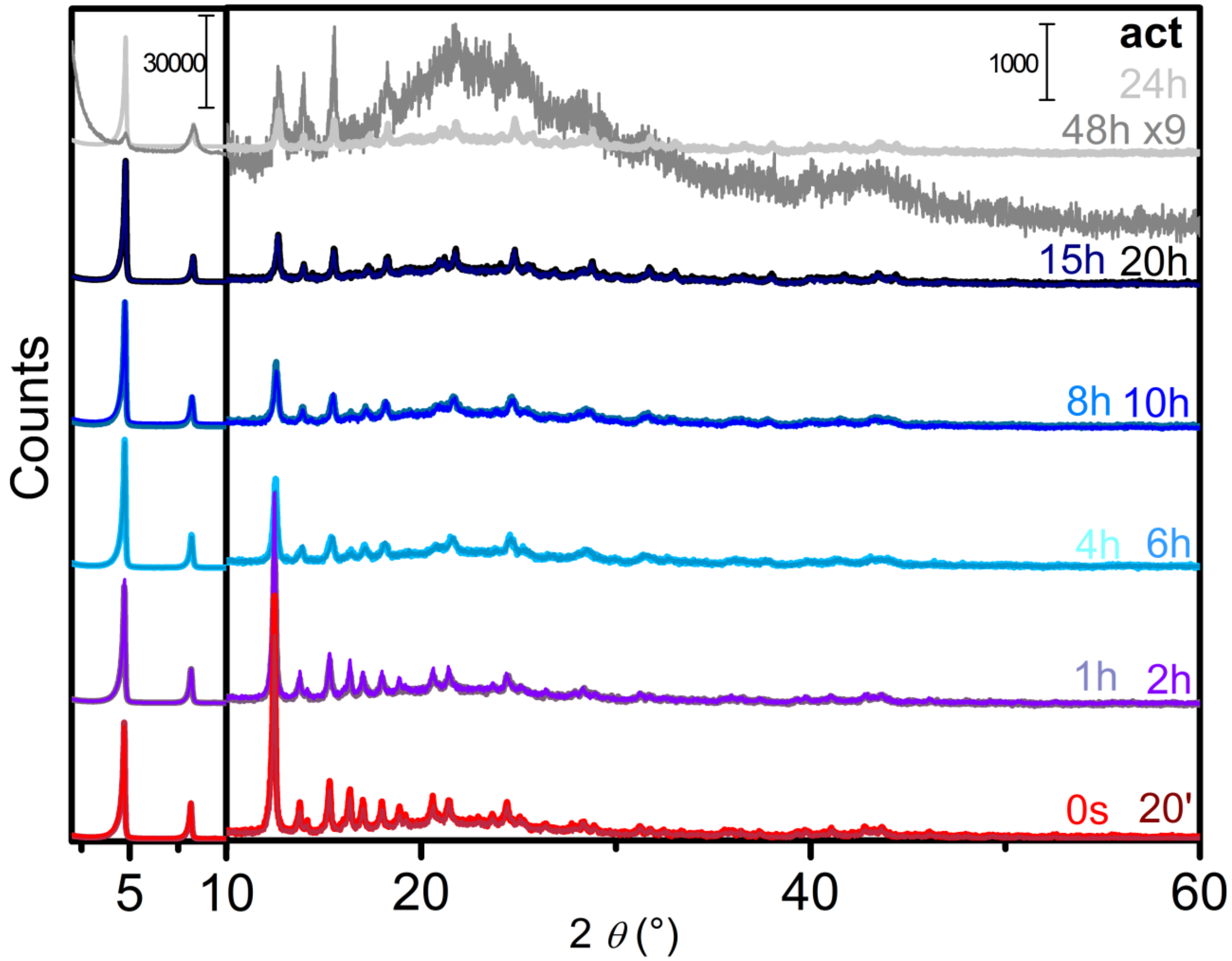

Figure S5. In situ XRD patterns recorded over time for Mg_2(dobpdc) activated at 180°c for 15 h (**act**) and after exposure to air (22°C, 29-40 RH%) up to (**act-indoor**). The pattern recorded after exposure for 48 h is also reported.

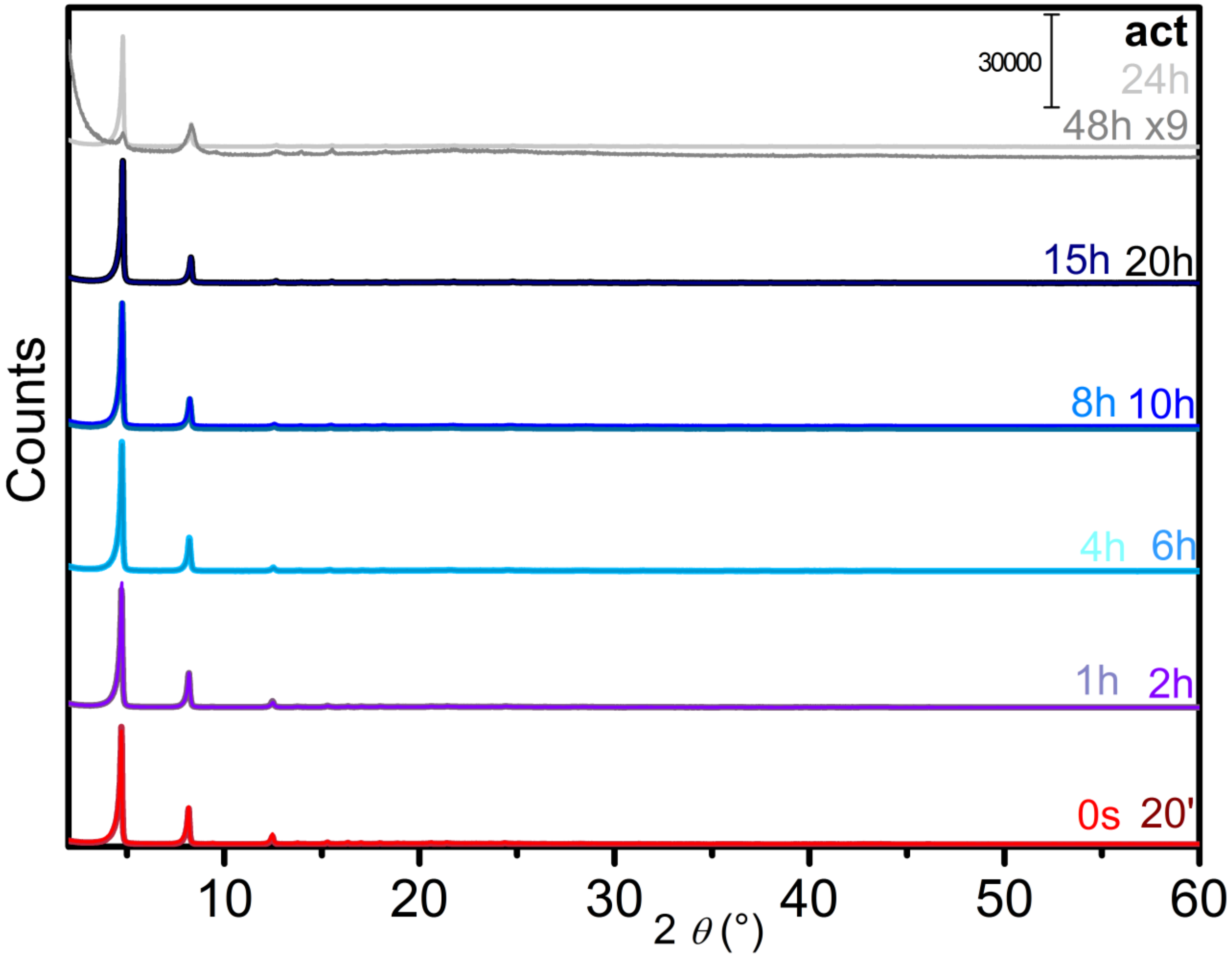

Figure S6. In situ XRD patterns reported in Figure S5 by adopting the same scale in the whole angle range.

S5. Ex situ XRPD measurements

The patterns reported in Figure 1 in the main text are reported in Figure S7 by adopting the same scale in the whole angle range to allow appreciating the different intensity of the bands.

It is evident that the patterns collected for the **sol** samples are significantly less intense than for the **act** samples. This difference is in part associated to an easier packing of the powder in the capillary if dry. Nevertheless, the intensity is almost the same for the peaks at $2\theta > 15°$. The higher intensity of the **act** pattern can be then related to a the lower electronic density in their pores, that is due to a lower degree of solvation. No significant changes are observed in the patterns before and after the aging in all cases. For what concerns the **act-indoor** sample, the in situ XRPD study evidenced a small increase in the peak intensity up to 4 h (azure line in Fig. S5). After this time, a shift of the peaks to higher angles is observed (of about 0.1° after 24 h) accompanied with a decrease in their intensity. This phenomenon is particularly evident for the peak at 12.6° (associated to the (210) reflections). The differences in the **act** and **act-indoor** patterns remained quite small: accordingly the N_2 and CO_2 adsorption measurements confirmed the retaining of the MOF structure after exposure to the atmosphere (see Table 1 and Fig. 2). For what concerns **sol-indoor**, an increase in the peaks intensity at low angles was observed during the first hour accompanied by a small shift to lower angles (see Fig. S3). These changes can be likely associated to evaporation of the excess methanol molecules from the MOF pores. After 2 h of air exposure, a reverse phenomenon started, similarly to what observed for **act-indoor**, with a decrease of the peak intensity and a shift towards higher angles. After 20 h, all the peaks were shifted to higher angles for less than 0.1°, decreasing in intensity for more than the 20%. The only exception was the peak at 4.7°, increasing of intensity of 26% with respect to the starting pattern. Nevertheless, the difference between the **sol** and **sol-indoor** patterns remained quite small and did not portend the 93% decrease in surface area of **sol-**

indoor (see Table 1). This confirms what recognized in the MOF literature that surface area measurements are more effective than diffraction in evaluating the materials integrity.[4] If a higher RH% is considered (**humid** samples), a strong decrease in porosity was observed (>80%) for both **sol** (dark blue line in Fig. 2) and **act** (violet line) samples. Nevertheless, also in this case the preactivated sample still showed a higher stability (see Table 1). It is surprising that a lower structure loss was observed for **sol-humid** than for **sol-indoor**. This result was confirmed by XRPD measurements: the **sol-humid** pattern is in fact two times more intense than the **sol-indoor** and the **sol** patterns (see Figure S7). This can be explained on the less tendency to evaporate of the solvent filling the pores in presence of a water saturated atmosphere, allowing a slightly lower damaging of the sample at high RH%.

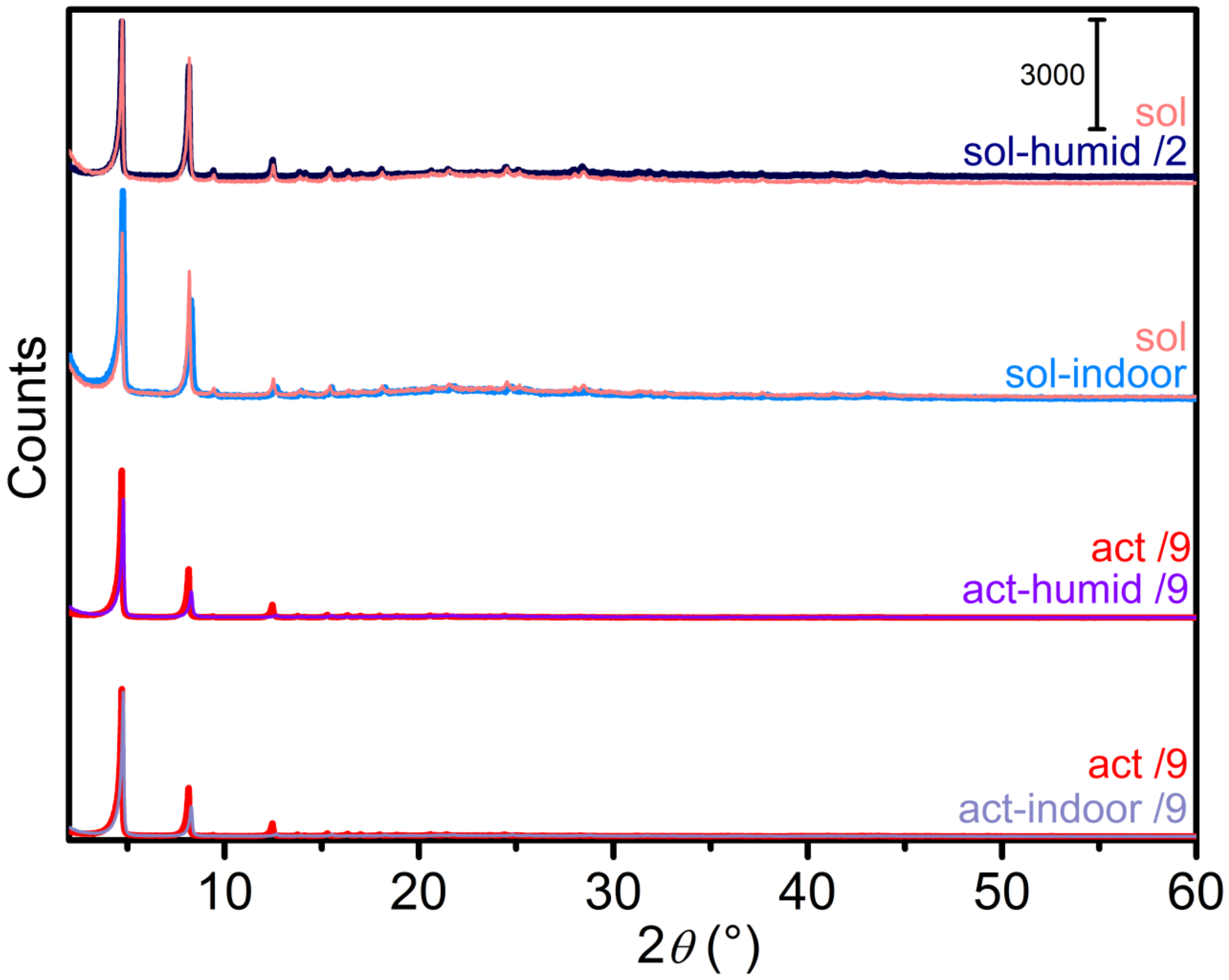

Figure S7. Ex situ XRD patterns of **act** and **sol** samples after exposure to air at 22-25°C and 29-40 RH% (**act-indoor**, light violet line; **sol-indoor**, blue line) or >86 RH% (**act-humid**, violet line; **sol-humid**, dark blue line) for 24 h. The pattern of the pristine **act** (red line) and **sol** (light blue line) samples are reported for comparison.

S5.1 Pawley refinement

The cell parameters of all the samples considered in these study have been obtained through a Pawley refinement of the patterns reported in Figure 1 of the main text and in Figure S7.

The cell volumes have been reported in Table S1.

The observed and calculated patterns as obtained by the Pawley refinement are reported in Figure S8.

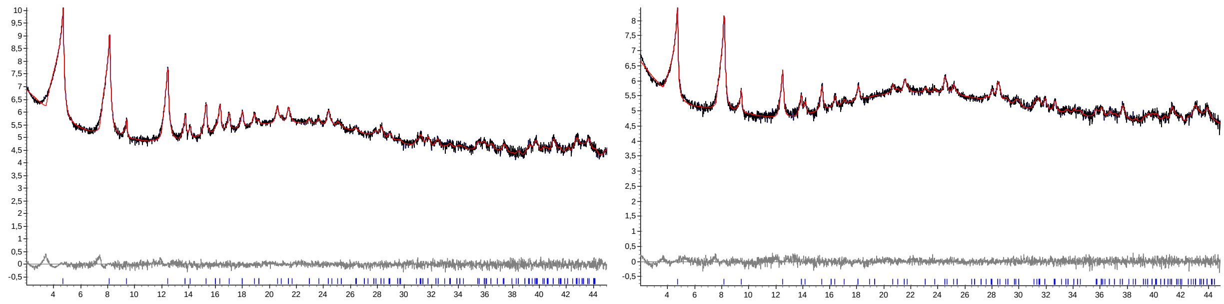

act

sol

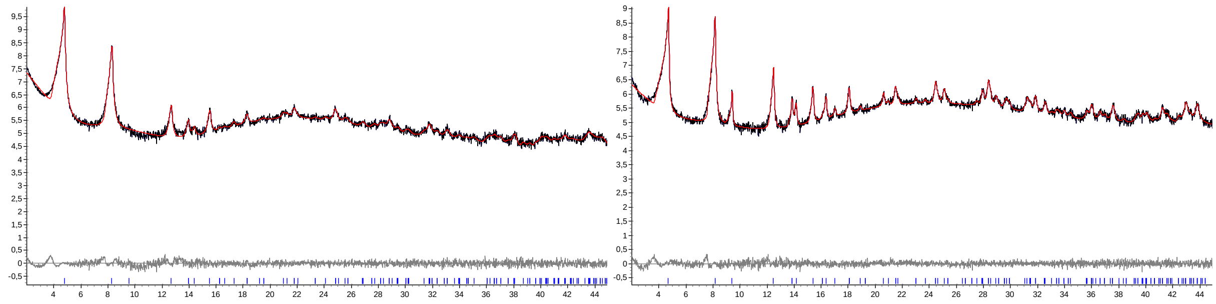

act-humid

sol-humid

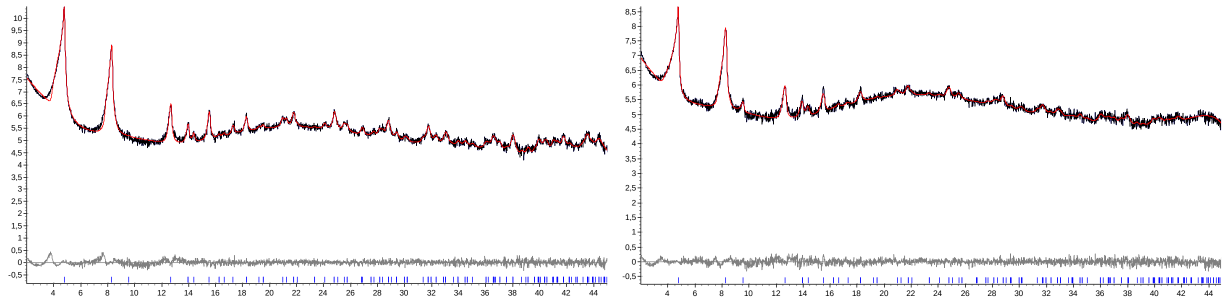

act-indoor

sol-indoor

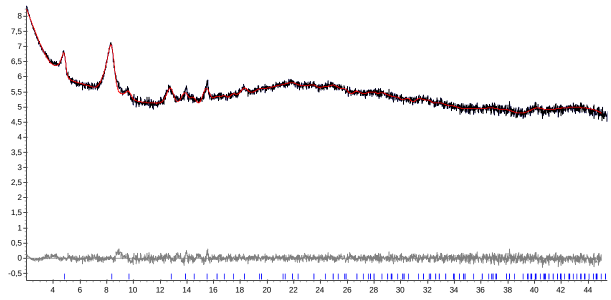

act-indoor after 48h

Figure S8. Observed (black lines) and calculated (red lines) diffraction patterns and final difference curve (grey lines) from Pawley refinements of all the samples. The experimental patterns used in the refinement have been those reported in Figure S7.

Table S1. *Cell parameters as obtained through Pawley refinement of the patterns reported in Figure 1.* $\alpha = \beta = 90°$, $\gamma = 120°$.

	a =b (Å)	***c (Å)***	***cell volume (Å³)***
act	21.7008(8)	6.847(1)	2792.2(5)
act-indoor	21.319(3)	6.749(1)	2657(1)
act-indoor-48h	21.0886(4)	6.773(3)	2613(5)
act-humid	21.302(1)	6.750(4)	2653(1)
sol	21.616(4)	6.782(2)	2745(1)
sol-indoor	21.315(5)	6.757(3)	2659(2)
sol-humid	21.671(1)	6.794(1)	2763.4(5)

S6. CO_2 adsorption isotherms

All the CO_2 isotherms measured at 25°C are reported in Figure S9. A small hysteresis is observed for all the samples, closing at low pressures indicating the full reversibility of the adsorption process. Nevertheless, although for the undamaged samples the hysteresis is in the error of the measurement (±10%), in all the other cases it is not. Two can be the causes at the origin of the hysteresis in Figure S9: (a) the chemical reaction of CO_2 with the oxidic defects in the material with the formation of carbonate- or bicarbonate-like species; (b) pore blocking due to structure collapse causing a more hindered diffusion of CO_2 molecules in the pores. The complete reversibility of the adsorption at RT and the results obtained by IR measurements, excluding the chemical reaction of CO_2 with the support (see Figure S11a) validate (b) as the most likely hypothesis.

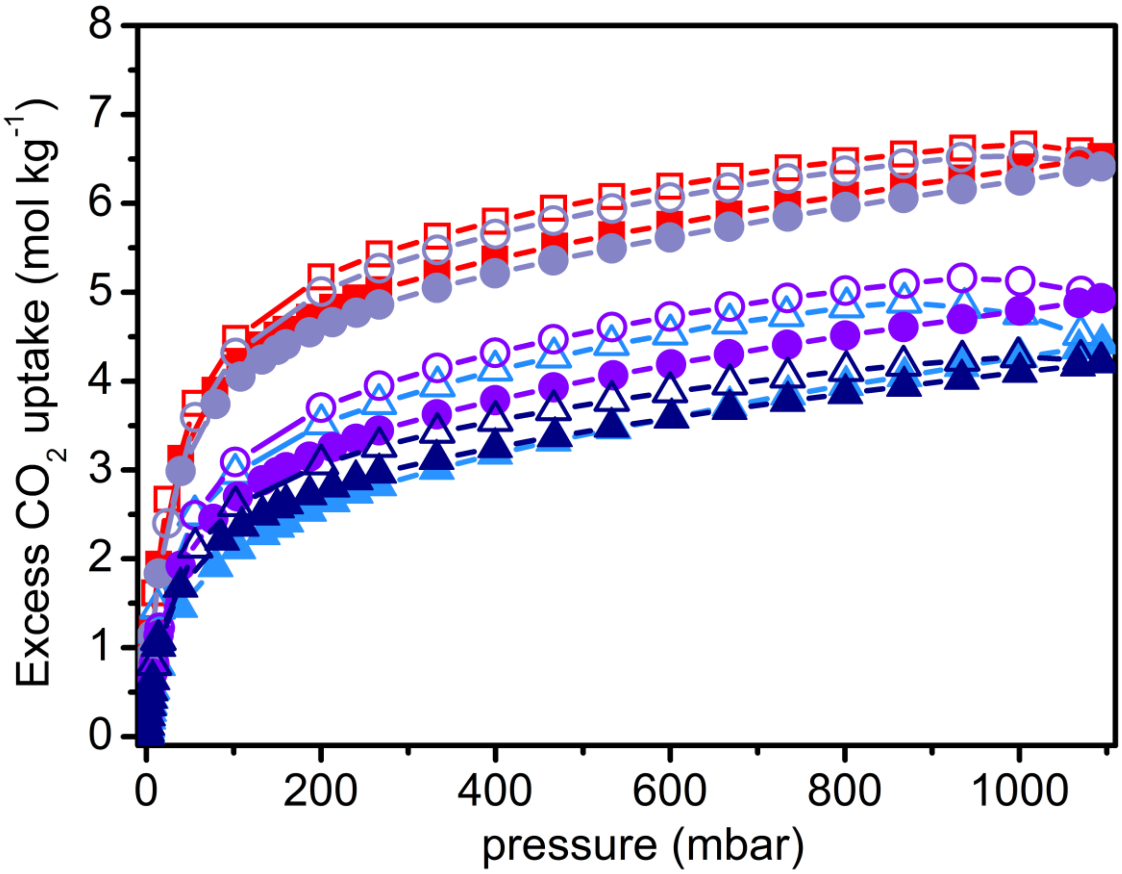

Figure S9. CO$_2$ adsorption isotherms at 25°C for **act** (circles, red), **act-indoor** (circles, light violet), **act-humid** (circles, violet), **sol-indoor** (triangles, light blue) and **sol-humid** (triangles, dark blue). Filled and empty scatters refer to adsorption and desorption points, respectively.

S7. Volumetric measurements of N_2 at 77 K

The experimental N_2 isotherms obtained at 77 K on act, sol and act-humid are shown in Figure S10. The surface areas obtained from the analysis of these isotherms are reported in Table S2. The act and act-humid have been treated at 180°C for 15 h before measurements, whereas the sol sample was degassed at RT.

The capping of all the Mg^{2+} with a methanol molecule causes a decrease of the surface area of about the 40%, whereas the degradation causes a decrease of 80%. This means that the decrease in the surface area observed for the degraded samples cannot be associated only to the capping of Mg^{2+} by –OH species but it has also to be associated with a partial structure loss.

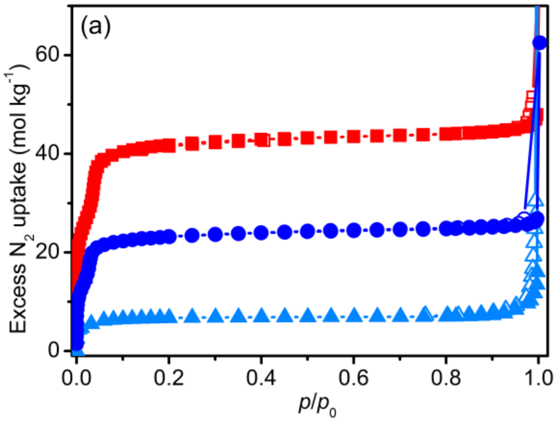

Figure S10. N_2 isotherms at 77 K and on act (squares, red line), sol (circles, blue line) and act-humid (triangles, light blue line). The full and empty scatters refer to the adsorption and desorption branches, respectively.

Table S2. Experimental Langmuir and BET surface area for act, sol and act-humid.

	S_{BET} (m^2 g^{-1})	S_{Lanmguir} (m^2 g^{-1})
act[a]	2941	3895
sol[a]	1761	2332
act-humid[a]	513	680

[a] Standard range of pressure considered in the fit for the surface area $0.05 < p/p0 < 0.2$.

S8. FTIR spectroscopy

FTIR spectroscopy was adopted as technique to investigate the nature of the defects created in the MOF after the reaction with atmospheric moisture and to evidence which are the sites responsible for CO_2 adsorption in the damaged sample.[5] In general the decomposition of MOFs characterized by metal-oxygen bonds is accompanied by the creation of hydroxyls in correspondence of the defects, visible in the IR spectra essentially as signals in the 3700-3300 cm^{-1} region.[6, 7] Two samples were prepared. In one case, the activated pellet was contacted with 20 mbar of H_2O for 1 hour (equilibrium pressure). Subsequent dosages of vapor were done in the first 5 min in order to fully hydratate the MOF (**act-humid**). The material was then reactivated in vacuum for 1 h at RT and then for 15 h at 250°C. The prolonged degassing at RT before the heating ramp was done in order to avoid an eventual further decomposition due to MOF exposure to water vapor at temperature higher than 100°C.[7] Another sample was prepared by contacting the activated pellet with a saturated pressure of methanol and then exposed to air (**sol-indoor**). The material was then reactivated in vacuum for 1 h at RT and then for 15 h at 250°C. The spectra obtained for the two samples were identical and then only the results for **sol-indoor** have been reported (dark blue spectrum in Figure S11a and b).

S8.1 Defect sites

As an effect of the damaging on the IR spectra, a decrease in the intensity of about 20% was observed for all the IR peaks with respect to the act ones (see in particular Figure S11b). Moreover, two broad signals appeared in the hydroxyl region, at 3605 and 3288 cm^{-1}, corresponding to free and bonded –OH, respectively,[8] as can be appreciated in the spectra recorded in transmission (Figure S11a). These bands cannot be associated to adsorbed water, being the relative signals observed at significantly different frequencies, as can be appreciated in the spectrum obtained for **act** in contact with 0.4 mbar of water (light azure curve in Figure S11a). The low intensity of the

–OH bands can be due to a partial condensation of the hydroxyls during activation. Only few isolated –OH groups would remain in the material after activation (band at 3605 cm^{-1}). For what concerns the band at 3288 cm^{-1} it corresponds to –OH groups involved in H-bonds that is known to cause a decrease in the peak intensity and in an increase in their FWHM. The intensity of the hydroxyls signals is quite low, compared to the corresponding decrease in the surface area observed from **act** (light blue spectrum in Figure S11a) to **sol-indoor** (dark blue curve) (about 90%). Besides the hydroxyls bands, only slight changes are observed in the spectrum (disappearance of a peak at 1010 cm^{-1} and appearance of a shoulder at 763 cm^{-1}). No signals are visible related to the formation of carbonate/bicarbonate-like species, associable with a possible reaction of the material with atmospheric CO_2 (see Figure S11). All the other MOF bands are essentially unchanged after exposure to a water saturated atmosphere. This is agreement with what reported by Tan et al.[7] on MOF-74-Mg decomposition. In this study, the combination of FTIR and quantum mechanical calculations has allowed to describe the processes at the basis of MOF-74 decomposition. In particular, the first step of this process would consist in the dissociation of a water molecule coordinated to Mg^{2+} with the formation of a Mg-OH and the corresponding protonation of the oxygen of the linker, in particular of the oxygen of the alcoholate, leaving the carboxylate group in its anionic form. This would explain the absence of signals that can be associated to carboxylic groups in the damaged material. The absence of the bands associated to –OH species in the 3600-3300 cm^{-1} region in the spectra reported in Ref. 7 is due to the different modality used for the spectra acquisition (a pressed powder on a KBr pellet), that allows to observe the phonon modes in scale but has as drawback a low sensitivity, making difficult the observation of the bands having a low intensity. In this study, it is also demonstrated that the Mg-OH group would be responsible of the appearance of the band at 763 cm^{-1} (bending mode) whereas the –OH group on the linker would give a signal located at 1333 cm^{-1} but, because of the strong coupling with the MOF phonons, is not observable.[7]

The mechanism described in Ref. 7 would explain for MOF-74-Mg on one hand the small changes in IR and Raman spectra and in XRD patterns before and after the exposure to air (indicating that the MOF structure is maintained at least in the first phases) and the lowering of the CO_2 uptakes observed in IR spectra (suggesting a lower availability of the open Mg2+ sites in the damaged samples). Nevertheless, although this can explain the small changes in the IR and XRD results from **act** to the damaged samples here reported for Mg_2(dobpdc), a simple capping of part of the Mg^{2+} species cannot explain completely the drop in surface area observed from **act** to any of the decomposed materials. In fact, if the Mg^{2+} ions are fully capped with methanol molecules, in this case the surface area decreases from 3895 to 2332 m^2 g^{-1} (see Section S7 and Table S2) whereas the surface area of decomposed materials drop to values lower than 700 m^2 g^{-1} (see Table 1). For Mg_2(dobpdc), the decrease of the MOF surface area after decomposition have to be associated to a partial structure collapse. See Section S9 for more details.

S8.2 CO_2 and N_2 adsorption

The nature of the CO_2 adsorption sites in the damaged samples was also investigated by means of FTIR spectroscopy. In Figure S12 (part a), the IR spectra are reported in the CO_2 asymmetric stretching band region as obtained after contact of 1 mbar of CO_2 with **act** (red spectrum) and **sol-indoor** (light blue spectrum). The position of the CO_2 asymmetric stretching band at low coverage in the two sample was the same (at 2354 cm^{-1}), suggesting Mg^{2+} as the main adsorption sites[9] in both the damaged and the undamaged samples. Only a slight decrease in the accessible Mg^{2+} concentration was suggested upon degradation because of a decrease in the IR intensity of about 1/3. In order to verify if CO_2 was able to react with defects, 40 mbar of CO_2 were dosed on **sol-indoor** at RT. After CO_2 dosage, the hydroxyl signals do not move suggesting that at this pressures the probe molecule is not interacting with them (green curve in Figure S11a). Moreover, besides the bands associated with molecular CO_2, no other signal appears in the spectrum, in particular in the 1670-1300 cm^{-1} region, region characteristic of carbonate and bicarbonate-like species. This region is only partially covered by MOF framework modes and then the chemical reaction of CO_2 with the support can be reasonably excluded at these pressures and this excludes it as a reason of the hysteresis observed in the isotherms of Figure S9.

A similar experiment was carried out for N_2 by dosing 40 bar of gas at RT on the **act** and the **sol-indoor** samples and then lowering the temperature to 77 K (part b of Figure S12, final pressure: 11 mbar). Also in this case the same position of the infrared stretching mode of N_2 was observed in the two samples upon adsorption, indicating that the probe molecule was coordinated to the same adsorption sites. From the position of the band, the adsorption sites were identified in both cases with open Mg^{2+} sites.[9] In this case, 11 mbar of nitrogen was chosen as pressure because the volumetric measurements indicated that the gas uptake by the sample is definitely larger than the one necessary to saturate the Mg^{2+} sites (6.26 mol kg^{-1}, see Figure 1). N_2 stretching mode is IR inactive in the gas phase and after adsorption with apolar surfaces, whereas it becomes activated in the Mg_2(dobpdc) only after coordination by very polarizing sites (as Mg^{2+}). The relative intensity of the N_2 band in the two samples can then used to estimate the percentage of Mg^{2+} still available to the interaction after material damage. Also in this case, about 2/3 of the Mg^{2+} seem to be still available to the interaction after damaging, in accordance with the results obtained by CO_2 adsorption, both by means of infrared spectroscopy and volumetry. This means that, although the adsorption sites are the same in the damaged and in the undamaged materials, the decrease in the surface area causes an apparent increase in the affinity of the material (see Figure 3). A more detailed characterization of the damaged material by IR spectroscopy has been addressed in another study.[10]

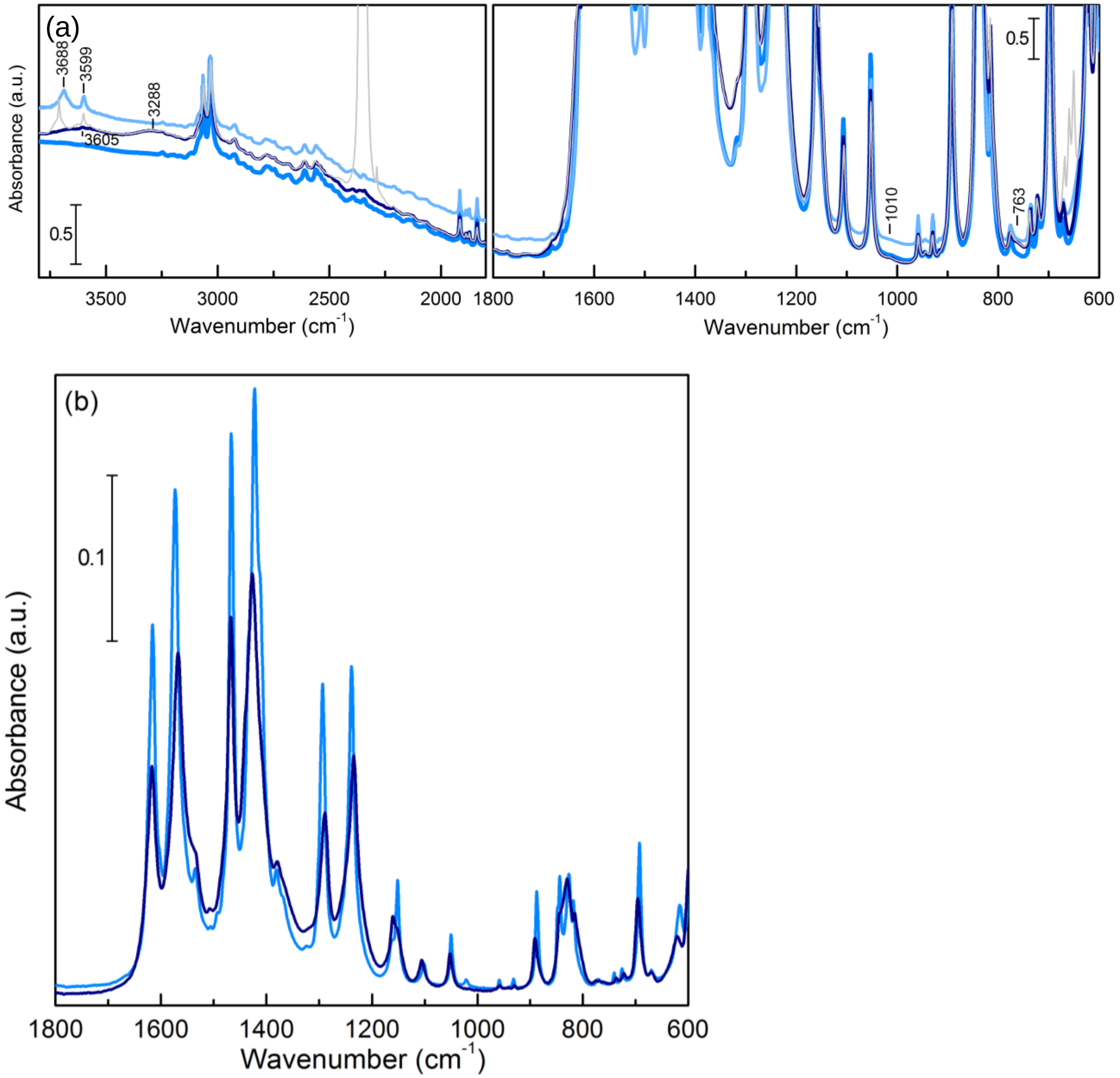

Figure S11. FTIR spectra recorded (a) in transmission and (b) in ATR for activated Mg_2(dobpdc) (**act**, azure) and a reactivated moisture damaged sample (**sol-indoor,** dark blue). A spectrum of **act** in contact with 0.4 mbar of H_2O is reported for comparison (light azure). The grey line in part (a) refers to activated **sol-indoor** in contact with 36 mbar of CO_2.

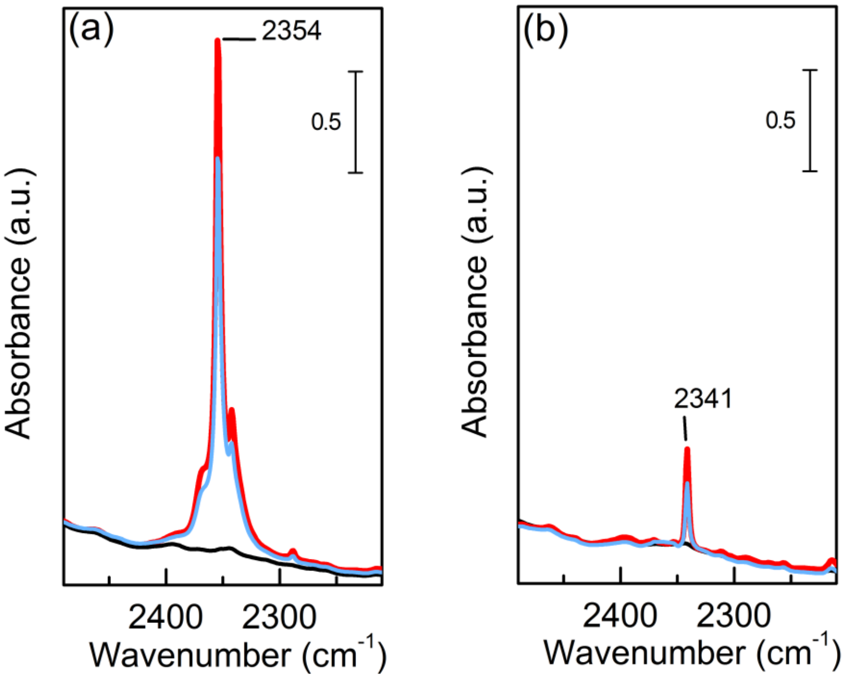

Figure S12. IR spectra recorded for activated Mg_2(dobpdc) (**act**, red line) and the reactivated moisture damaged sample (**sol-indoor**, light blue line) after contact with (a) 1 mbar of CO_2 at RT or (b) 11 mbar of N_2 at 77 K. As black line the spectrum of the activated **sol-indoor** sample is reported.

S9. Hypothesis on the Mg_2(dobpdc) structure after degradation

Although outside the aim of the present paper, a possible mechanism of Mg_2(dobpdc) decomposition in the steps following the formation of Mg-OH and C-OH species was hypothesized on the basis of the results obtained and it is schematized in Figure S13, hypothesizing a larger damaging along (a) the (001) or (b) the (010) and (100) directions. The latter possibility would found a confirmation in the small changes observed in the XRD patterns reported in Figure 1. In Figure S14 the first step of the decomposition mechanism, accordingly to the mechanism described in Ref. 7, is schematized. Material damaging was accompanied in all cases by a change in color of the material, as reported in Table 1 and in Figure S2. The coloring can be associated to the creation of defects in the Mg-O-Mg filars or to the formation of small MgO (or $Mg(OH)_2$) clusters due to partial structure loss.[11-14] This change in color can be also associated to the creation of a semiquinone state (that is blue) due to a partial O_2 sensitivity. Nevertheless, the green color was also observed after exposure of the material to a pure water atmosphere, allowing to consider the O_2 sensitivity in the conditions adopted, if real, as a secondary process. It is interesting that the color was retained in presence of air, in general causing the disappearance of the coloration in Mg-O based materials when their coloration is associated to the presence of color centers. As mentioned in the main text, in this case the color disappeared only when the RH was higher than 60%. The presence of these clusters was not evidenced in XRPD patterns, where no new peak appeared after aging and in particular at 38° and 43°, that is in regions relative to the most intense reflection for crystalline $Mg(OH)_2$ and MgO, respectively (see Figure S7). Nevertheless, the presence of these clusters cannot be ruled out on the basis of XRPD measurements because the dimension of these clusters could be under the detection limit of XRD. A high concentration of Mg-OH species (typical of nanometric MgO and $Mg(OH)_2$) was ruled out also by IR spectroscopy.

The spectrum obtained for **sol-indoor** is reported as an example in Figure S8 (dark blue curve). Two broad bands associated to hydroxyls appear in the MOF spectrum after damaging at 3605 and 3288 cm^{-1}, that is at lower wavenumbers than those typical of Mg-OH species.[15, 16] MgO nanoclusters fast react with atmospheric water and CO_2[15] and the formed Mg-OH species can be dehydrated only at temperatures higher than 300°C. [15] This allows to rule out also the presence of MgO clusters in the pores. Moreover, CO_2 dosing on activated **sol-indoor** does not evidence the formation of carbonate or bicarbonate-like species (green curve in Figure S11a), further supporting the hypothesis of the absence of these species in the MOF pores. The position of the CO_2 and N_2 stretching band in IR spectra in **sol-humid** was observed at the same position than for **act** (at 2354 and 2341 cm^{-1}, respectively, as discussed above, see Figure S12) although a lower intensity of the peak was observed for the damaged sample (about 2/3 than for **act**). This would indicates open Mg^{2+} as the main adsorption sites in both the damaged and the undamaged samples. Only a slight decrease in the accessible Mg^{2+} concentration is observed, likely because of the lability of the –OH couples at the temperature used in the material activation, allowing to restore, at least partially, the open Mg^{2+} sites. Then, the decrease in the surface area cannot be associated to the formation of $MgO/Mg(OH)_2$ nanoclusters but to a partial structure collapse (see Figure S13 for some possible degradation mechanism). The lower decrease of the CO_2 uptake with respect to the N_2 ones upon degradation indicated by volumetry would be then explained by the different temperature at which the two adsorptions were carried out (RT and 77 K, respectively). In fact, whereas N_2 condensates in the MOF pores at 77 K, allowing to evidence the changes in the MOF structure, CO_2 at RT and 1 bar is probing only the Mg^{2+} sites, as testified by the uptake almost coincident with the one expected for the saturation of the open metal sites (6.26 mol kg^{-1} in the act sample). CO_2 would not be too sensitive to changes in the MOF structure.

The small changes in XRD patterns after aging would validate this hypothesis. Moreover, the N_2 isotherms before (red curve in Figure 2) and after the exposure to air maintain a IIb type, not showing the appearance of a hysteresis loop. This excludes an important formation of mesopores, in general accompanying structure degradation in microporous materials. The significant decrease in surface area upon aging could be then explained by a frequent pore blocking due a localised collapse of the MOF structure that in some cases can be also seen as a fragmentation of the single MOF crystals (Figure S13a amd second path in Figure S13b). The color associated to degradation would be then due to the creation of defects in the Mg-O-Mg filars.

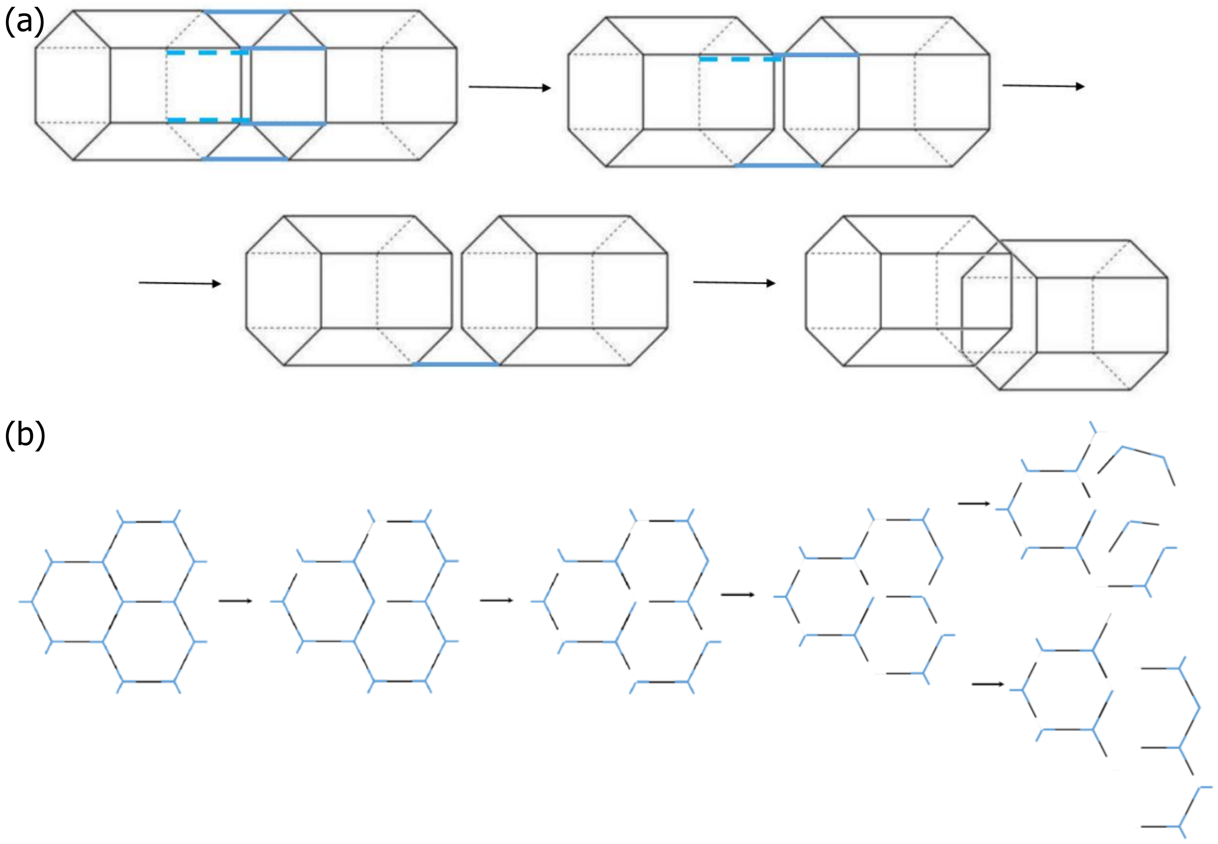

Figure S13. Pictorial representation of possible degradation mechanisms in Mg_2(dobpdc) on time. The blue segments represent Mg-O bonds. In (a) the mechanism is illustrated using a crystal constituted by a single channel where the hexagonal prism represent two parts of a MOF channel. The decomposition is supposed to happens mainly along the (001) direction. In (b) the crystal is view along the (001) direction considering three neighbor channels and in this case the decomposition is hypothesized mainly along the (100) and (010) directions. After that the number of hydrolised Mg-O bonds is higher than a threshold amount, rearrangement of portion of the MOF pores can rearrange resulting in pore blocking. A possible mismatch of two parts of a channel can also happen with consequent pore blocking and decrease in the surface area. Such a change, being essentially a change in local environment of Mg due to Mg-O bond hydrolysis described in Figure S14, would not be strongly evident in IR and XRD measurements but it would detectable only by N2 volumetry at 77 K.

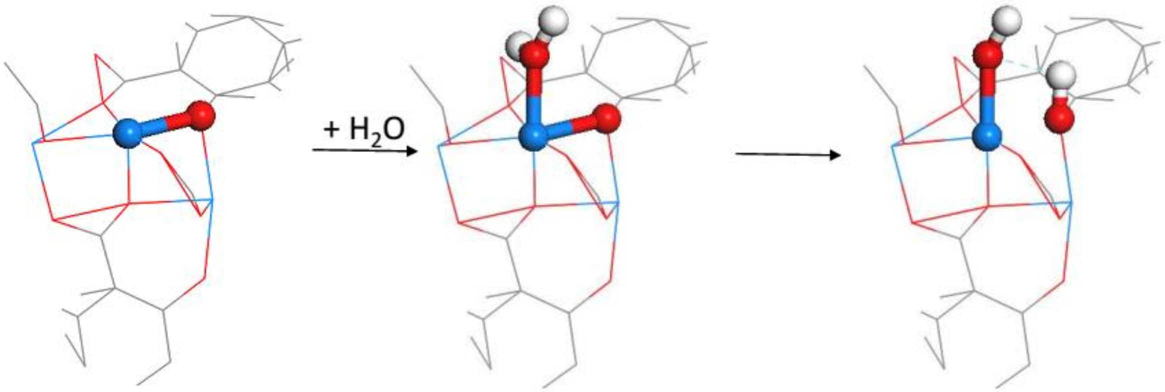

Figure S14. Pictorial representation of the first step of the degradation of Mg_2(dobpdc) accordingly to the mechanism reported by Tan et al.[7] Atoms are represented with the following color code: Mg (blue), O (red), C (grey), H (white).

REFERENCES

1. D. Gygi, E. D. Bloch, J. A. Mason, M. R. Hudson, M. I. Gonzalez, R. L. Siegelman, T. A. Darwish, W. L. Queen, C. M. Brown and J. R. Long, *Chem. Mater.*, 2016, **28**, 1128-1138.
2. S. J. Gregg and K. S. W. Sing, *Adsorption, surface area and porosity (2nd ed.)*, Academic Press Inc., London, 1982.
3. I. Langmuir, *J. Am. Chem. Soc.*, 1918, **40**, 1361–1403.
4. P. M. Schoenecker, C. G. Carson, H. Jasuja, C. J. J. Flemming and K. S. Walton, *Ind. Eng. Chem. Res.*, 2012, **51**, 6513-6519.
5. K. Tan, N. Nijem, Y. Gao, S. Zuluaga, J. Li, T. Thonhauser and Y. J. Chabal, *Cryst. Eng. Comm.*, 2015, **17**, 247-260.
6. F. Bonino, C. Lamberti, S. Chavan, J. G. Vitillo and S. Bordiga, in *Metal Organic Frameworks as Heterogeneous Catalysts*, eds. F. Llabrés i Xamena and J. Gascon, RSC Catalysis Series, Cambridge, 2013, pp. 76-142.
7. K. Tan, S. Zuluaga, Q. Gong, P. Canepa, H. Wang, J. Li, Y. J. Chabal and T. Thonhauser, *Chem. Mater.*, 2014, **26**, 6886-6895.
8. N. B. Colthup, L. H. Daly and S. E. Wiberley, *Introduction to Infrared and Raman Spectroscopy (Third Edition)*, Academic Press, San Diego, 1990.

9. L. Valenzano, B. Civalleri, S. Chavan, G. Turnes Palomino, C. Otero Areán and S. Bordiga, *J. Phys. Chem. C*, 2010, **114**, 11185-11191.
10. J. G. Vitillo et al., *J. Phys. Chem. C*, 2016, in preparation.
11. M. Heyde, G. H. Simon and L. Lichtenstein, *Phys. Status Solidi B*, 2013, **250**, 895-921.
12. P. Rinke, A. Schleife, E. Kioupakis, A. Janotti, C. Rödl, F. Bechstedt, M. Scheffler and C. G. Van de Walle, *Phys. Rev. Lett.*, 2012, **108**, 126404.
13. M. Sterrer, M. Heyde, M. Novicki, N. Nilius, T. Risse, H.-P. Rust, G. Pacchioni and H.-J. Freund, *J. Phys. Chem. B*, 2006, **110**, 46-49.
14. H.-R. Zhang, R. Egerton and M. Malac, *Nucl. Instrum. Meth. Phys. Res. B*, 2013, **316**, 137-143.
15. D. Barthomeuf, *Catal. Rev.*, 1996, **38**, 521-612.
16. A. A. Tsyganenko, *J. Struct. Chem.*, 1975, **16**, 536-540.